Predicting the flow field inside a close-coupled catalyst - the effect of entrance losses

Benjamin, S.F. , Zhao, H. and Arias-Garcia, A.

Original citation & hyperlink:
Benjamin, S.F. , Zhao, H. and Arias-Garcia, A. (2003) Predicting the flow field inside a close-coupled catalyst - the effect of entrance losses. Proceedings of the Institution of Mechanical Engineers, Part C: Journal of Mechanical Engineering Science, volume 217 (3): 283-288.
http://dx.doi.org/10.1243/095440603762870036

Predicting the flow field inside a close coupled catalyst-the effect of entrance losses.

S. F. Benjamin, H. Zhao, A. Arias-Garcia

School of Engineering, Coventry University, Coventry, UK

Abstract: A methodology is described for improving the prediction of the flow distribution in automotive close-coupled catalysts using computational fluid dynamics (CFD). Steady and pulsating flow simulations have been performed and compared with measurements obtained on an isothermal flow rig. By incorporating an extra pressure loss due to oblique entry at the monolith improved flow predictions are obtained. This work extends the methodology which has previously been developed for axi-symmetric systems.

Keywords: flow maldistribution, catalytic converters, CFD, entrance effects

NOTATION

k	turbulent kinetic energy
n	iteration number
ΔPe	entrance total pressure loss
Re	Reynolds number (inlet pipe)
W	Inlet velocity
v_r, v_c, v_z	radial, circumferential and axial velocity components

ε dissipation rate of turbulent kinetic energy

ρ air density

1 INTRODUCTION

Maldistributed flow in automotive exhaust catalysts can adversely affect system pressure loss and exhaust emissions. It can also lead to premature catalyst deactivation. Hence a simulation technique which can predict flow distribution is highly desirable. Computational fluid dynamics (CFD) is now widely used in the automotive industry when designing autocatalyst systems. However demonstration of accurate flow prediction is clearly necessary if confidence in the technique is to be established. In previous studies [**1,2**] it was shown that CFD generally underpredicted the flow maldistribution in both axi-symmetric and fully three-dimensional catalyst systems. The cause of such underprediction was identified as an inadequate description of the pressure loss experienced at the front face of the catalyst due to the obliqueness of the entry flow. Benjamin et al [**3**] derived an expression for accounting for these losses in axi-symmetric converters based on the work of Küchemann and Weber [**4**] who were addressing the similar problem of oblique entry to flat plate heat exchangers. Axi-symmetric systems are fairly representative of underbody designs which normally comprise a single upstream exhaust pipe expanding via a diffuser into the catalyst monolith. With the move to tighter emission legislation the trend is now to position automotive catalysts close to the engine. These close-coupled catalysts (CCC) achieve rapid warm up and reduced light off times, thus lowering emissions considerably. Because of their positioning they are quite

different geometrically from typical underbody designs. CCCs usually feature individual exhaust pipes from each cylinder discharging into different locations in the diffuser. The geometry is thus quite complex, the flow highly three dimensional and strongly pulsating [**2**]. The objectives of this study are to extend the entrance methodology developed in [**3**] to CCCs and to compare predictions with experimental data obtained from a flow rig for both steady and pulsating isothermal flow conditions.

2 EXPERIMENTAL SETUP

The isothermal flow rig and measuring system have been previously described in [**2**]. Figure 1 shows a schematic of the flow rig and the configuration of the pulse generator. A constant mass flow rate was provided from a compressed air system with flow rate monitored by a viscous flow meter. The working section comprised of an inlet duct, CCC manifold, monolith and outlet sleeve. A contraction nozzle provided a 1D uniform velocity profile under steady flow conditions. Immediately downstream of the nozzle is the pulse generator comprising a rotating plate with holes encased in a housing. The plate interrupts the flow four times per revolution. Under pulsating conditions flow straighteners are required downstream of the generator in a supply pipe to provide a uniform velocity profile [**2**]. For a particular experiment individual ports of the CCC manifold were coupled to the end of the supply pipe, the other three being blanked off. The supply pipe diameter, on which all Reynolds numbers were based, was 48 mm. On the test substrate an outlet sleeve of length 32.5 mm was used to avoid entrainment of surrounding air.

The CCC from a 1.4 litre engine features four exhaust ports entering a diffuser (chamber) upstream of the monolith (see figure 2). The length and diameter of the cylindrical ceramic monolith are both 120mm. The monolith is comprised of about 7000 straight parallel channels with a nominal cell density of 62 cells/cm^2 (400cpsi). The hydraulic diameter of the channels is approximately 1mm and the monolith porosity 75%. The outlet nozzle from the production catalyst was replaced with a sleeve to facilitate velocity measurements at the rear of the monolith.

A TSI IFA 300 Constant Temperature Hot Wire Anemometry (HWA) system was used to measure the flow velocity at the rear of the monolith. The system comprises a main unit with the HWA bridges, a 2D traverse and the ThermalPro software to control, acquire and analyse the data. The probes were 5 μm Tungsten/Platinum wires, calibrated using a TSI 1129 fully automatic calibration rig. The velocity profiles were measured in the outlet sleeve 30 mm downstream of the monolith.

3 NUMERICAL SIMULATION

3.1 Model description

The CFD code STAR-CD was used [**5**]. The basic computational mesh is shown in figure 2. There are about 300,000 cells in the basic model. The mesh is composed of four parts, the manifold, the diffuser, the monolith and the exit volume. The monolith is modelled as a porous medium with a prescribed permeability and resistance. The exit sleeve is

represented as the last five layers of cells. All the velocity contour plots in this paper represent the position about 30mm downstream of the monolith exit. At the inlet port the flow was assumed uniform, only ports 1 and 2 were examined. An example of measured and approximated pulses for 25 Hz and Re ~70000 is shown in figure 3. These refer to a position in the supply pipe downstream of the flow straighteners. The inlet velocity is adequately approximated as sinusoidal pulsations. For the pulsating case described later port 1 was open and pulse frequency was 25Hz. Five cycles were simulated using 400 time steps (iterations) per cycle, each time step being 0.0001s. Inlet velocity was:

$$W = 44.76 + 35.81\left(\sin\frac{2\pi n}{400}\right)$$

where n is the iteration number. The mass flow rate was 0.044kg/s and the amplitude of the sinusoidal pulse 80% of the average, equaling 35.81 m/s. This velocity is higher than in figure 3 as a contraction was required between the circular inlet pipe and the oval shaped port of area 819 mm^2.

The standard k-ε model was used to solve for turbulence energy k and dissipation rate ε, and the algebraic law-of-the-wall was used to represent the boundary layer. The governing equations were discretised by either a first order up–wind (UD) or second order (MARS) scheme [**5**]. In the case of steady state flow, the finite-volume equations resulting from the discretisations were solved by the implicit SIMPLE algorithm [**5**]. In the case of pulsating flow, the PISO algorithm [**5**] was employed, and the case started from a converged steady state solution.

3.2 Monolith resistance

To resolve the flow details within each channel of the catalyst would require prohibitively large computing resources. A commonly used approach in CFD is to treat the monolith as a porous medium. Assuming the flow inside the channel is fully developed and laminar, the flow resistance in the monolith can be represented by choosing appropriate permeability coefficients in STAR-CD. Applying large transverse resistances in the monolith makes the flow uni-directional. The pressure drop along the monolith is normally described by the Hagen-Poiseuille equation as the channel Re is generally less than 1500. In reality, just upstream of the monolith the flow is far from unidirectional. In the case of close coupled catalysts, both swirl and radial velocity components will be found. Oblique entry at the channel inlet causes flow separation in the front part of the channel resulting in an extra pressure loss, termed the entrance effect. In [**3**] this was defined as

$$\Delta P_e = \rho v_r^2 / 2$$

where v_r is the radial flow component just upstream of the monolith. For the general case of non axi-symmetric flow the equivalent pressure loss expression becomes

$$\Delta P_e = \rho\left(v_r^2 + v_c^2\right)/ 2$$

where, v_r and v_c are the two non axial flow components just upstream of the monolith. For positive v_z this extra pressure loss was added to the monolith resistance within STAR-CD in a similar fashion to that as described in [**3**].

The basic model was run steady state for Re~60000 using the MARS scheme and then subsequently locally refined to reduce residual errors. Increasing cell numbers by 35% and subsequently 140% showed only small changes to the velocity distribution within the monolith and so a 35% refinement was considered adequate.

3.3 Test cases

Table 1 provides a summary of the test cases. Also shown are the maximum velocities in the monolith. For the steady flow cases Re~60000. When the entrance effect is included, a better match between prediction and experiment is achieved irrespective of the discretisation scheme. The higher order MARS scheme is also shown to be superior in terms of predicting maximum velocities.

3.3.1 Port 2, steady flow

Figure 4 shows the simulations for cases 1 and 2 compared with HWA measurements. Figure (4a) shows a crescent-shaped high velocity area encircling the centre of the monolith with a secondary band of high velocity at the periphery. On entry to the diffuser the flow separates and the emerging swirling jet impinges over a small section of the monolith. The locally high resistance results in a lateral pressure gradient forcing the jet to spread radially across the front face of the monolith. As this radial flow approaches the diffuser wall the pressure increases locally forcing more flow through the periphery. This is the origin of the secondary band of high velocity near the wall. The simulations

revealed a clockwise circulation which spreads these higher velocity regions in the swirl direction. In figure 4(b), the highest predicted velocity is 8.0 m/s about half of the measured velocity of 15.3 m/s. Including the entrance effect (figure 4(c) improves the prediction of maximum velocity to 10.6 m/s and also shows a clear distinction between the two high velocity regions.

The reason for the simulation improvement with the entrance effect is due to the redistribution of resistance across the monolith. Figure 4(d) shows contours of $\sqrt{\left(v_r^2 + v_c^2\right)}$ ($\propto \sqrt{\Delta P_e}$) at the front face of the monolith. The areas of increased resistance close to the central region are mainly associated with strong radial flow whilst that towards the periphery to swirl. These higher resistances serve to restrict entry into the monolith and redistribute the flow as shown in figure 4c. Redistributing the flow also increases the pressure drop across the monolith. Generally, for the steady flow cases the pressure drop is ~35 to 42% larger after introducing the entrance effect. In the pulsating case, the increase is about 46%.

3.3.2 Port 1, steady flow

Figure 4(e-g) show the results for cases 5 and 6. The outboard port provides more swirl. It seems that CFD has overestimated the swirl component which results in the clockwise shift of the intense flow area along the swirl direction. This is most likely due to inadequate prediction around the compound bend on the outboard port due to the inadequacies of the standard k-ε turbulence model. Incorporating the entrance effect

improves predictions of the maximum velocity which is now 10.8 m/s compared to a measured value of 11.1 m/s.

3.3.3 Port 1, Pulsating flow

Figure 5 shows that the pattern of flow under pulsating conditions is quite similar to that for steady flow. Again the simulation over-estimates the swirl. However, the prediction of the flow maldistribution has been improved after taking the entrance effect into account. The highest velocity increases from 9.7m/s to 11.1m/s, much closer to the measured value, 11.8 m/s. This is encouraging and suggests that the methodology may be applied to a full transient analysis of the system, a subject of ongoing research.

4 CONCLUSIONS

CFD simulations of the flow field inside a close coupled catalytic converter were conducted under steady and pulsating flow conditions and compared to experimental data obtained on an isothermal test rig. By incorporating entrance effects predictions of the maximum velocity within the monolith were substantially improved. This is important, as catalyst deactivation is believed to be closely associated with areas of high mass flow rate.

ACKNOWLEDGEMENT

The authors would like to acknowledge the support of ArvinMeritor and in particular Shoja Farr and Mick Worthington.

REFERENCES

1. **Benjamin S. F., Clarkson R. J., Haimad N. and Girgis N. S.(**1996) An experimental and predictive study of the flow in axi symmetric automotive exhaust catalyst systems **SAE Transactions, Vol. 105, Journal of Fuels and Lubricants,** Section 4, pages 1008-1019

2. **Arias-Garcia A, Benjamin S. F., Zhao H., and Farr S.**. A comparison of steady and pulsating flow measurements and CFD simulations in close coupled catalysts, SAE Paper No 2001-01-3662, 2001

3. **Benjamin S. F, Haimad N., Roberts C. A. and Wollin J,** Modelling the flow distribution through automotive catalytic converters, Proc Instn Mech Engrs, Vol 215, Part C, pp379-383

4. **Küchemann, D., Weber, J.**, Aerodynamics of Propulsion, McGraw-Hill Book Co. Inc., 1953

5. **Computational Dynamics**, STAR-CD Users Guide-Version 3.100A, 1999.

Table 1. Test cases.

Case	Flow	Port No.	Discretisation scheme	Entrance effect	Max Velocity m/s
1	Steady	2	MARS	No	8.0
2	Steady	2	MARS	Yes	10.6
3	Steady	1	UD	No	7.5
4	Steady	1	UD	Yes	8.9
5	Steady	1	MARS	No	8.4
6	Steady	1	MARS	Yes	10.8
7	Pulsating	1	MARS	No	9.7*
8	Pulsating	1	MARS	Yes	11.1*
Expt.	Steady	2			15.3
	Steady	1			11.1
	Pulsating	1			11.8*

*Cycle averaged.

List of Captions

Figure 1 (a) isothermal flow rig and (b) pulse generator.

Figure 2 Close coupled catalyst with basic computational mesh

Figure 3 Measured and sinusoidal flow pulsations, 25 Hz, Re~70000.

Figure 4. Velocity contours for steady flow, Re~60,000. (a) Port 2 HWA measurements, v_z, (b) Port 2 CFD case 1 without entrance effects, v_z, (c) Port 2 CFD case 2, with entrance effects, $v_{z,}$ (d) Port 2 CFD case 1, without entrance effects, $\sqrt{\left(v_r^2 + v_c^2\right)}$ (e) Port 1 measurements, v_z, (f) Port 1 CFD case 5, no entrance effects, v_z (g) Port 1 CFD, case 6 with entrance effects, $v_{z,}$ (h) View angle.

Figure 5 . Velocity contours with pulsating flow, 25Hz. (a) Port 1 HWA measurements, v_z, Re 72000 (b) Port 1 CFD case 7, without entrance effect, $v_{z,,}$ Re 69800 (c) Port 1 CFD case 8, with entrance effects, $v_{z,}$ Re 69800 (d) View angle

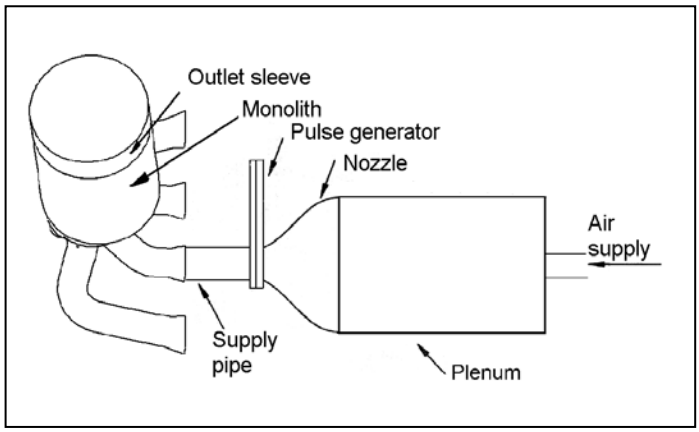

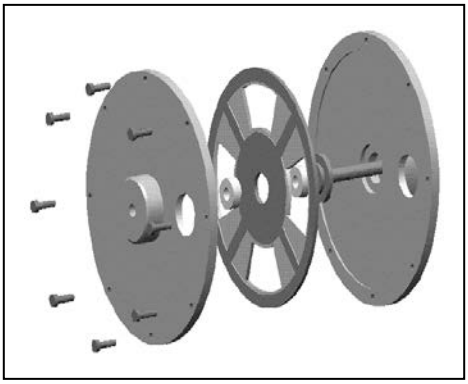

a b

Figure 1

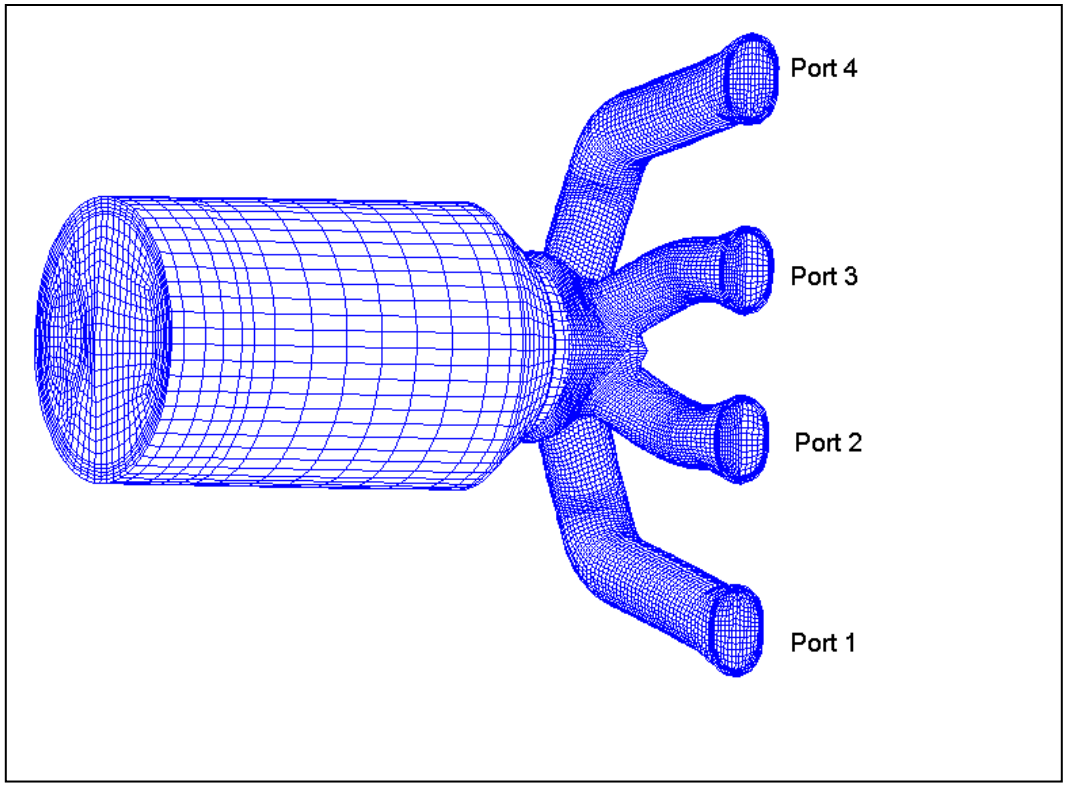

Figure 2

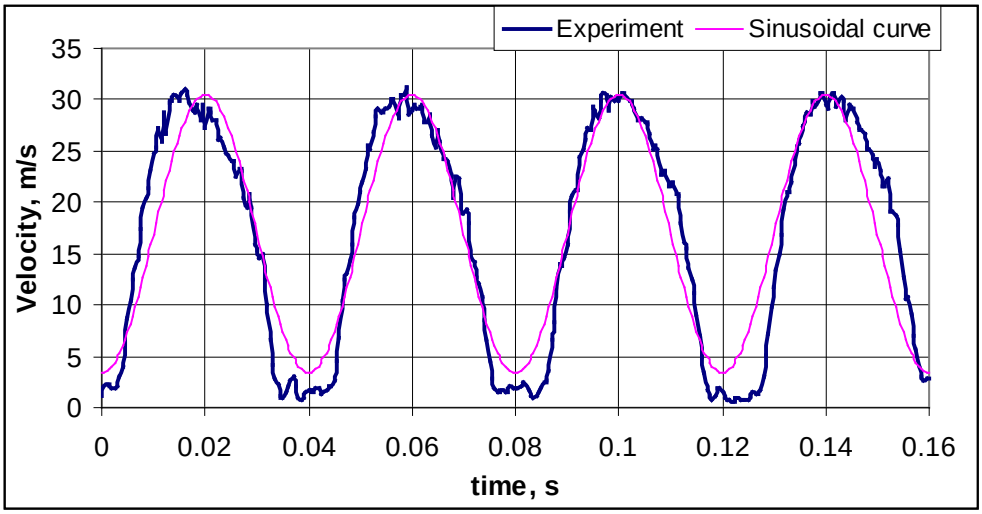
Experiment
Sinusoidal curve
Velocity, m/s
35
30
25
20
15
10
5
0
0
0.02
0.04
0.06
0.08
0.1
0.12
0.14
0.16
time, s

Figure 3

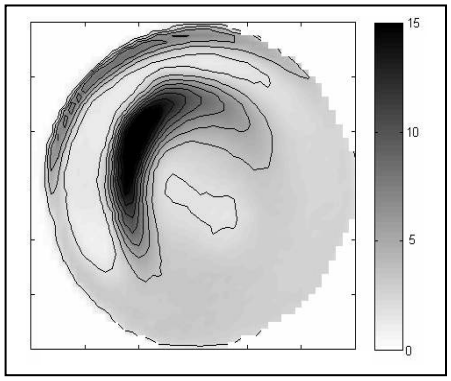

Fig 4a

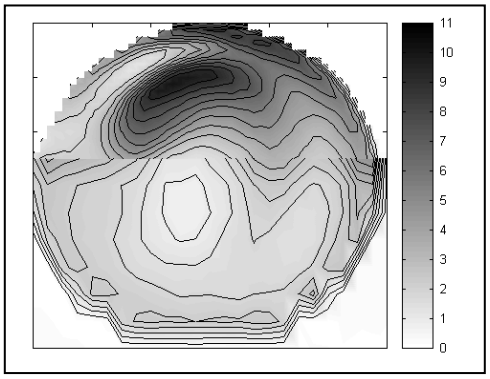

e

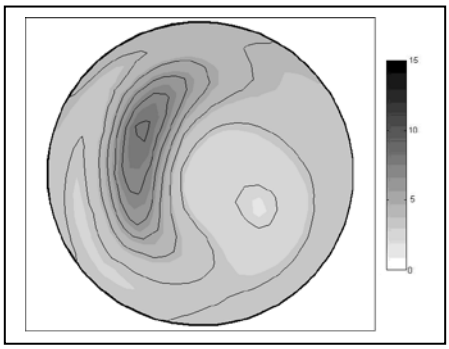

b

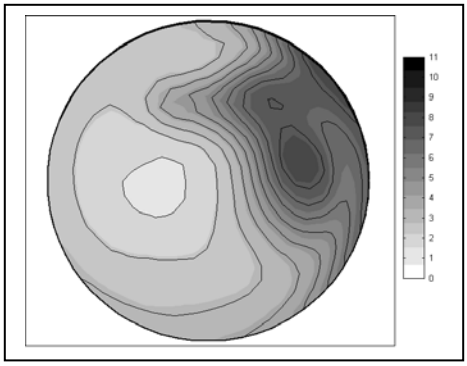

f

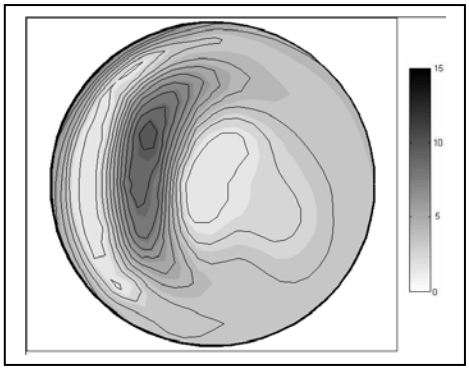

c

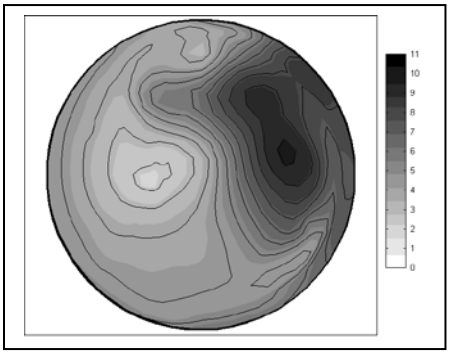

g

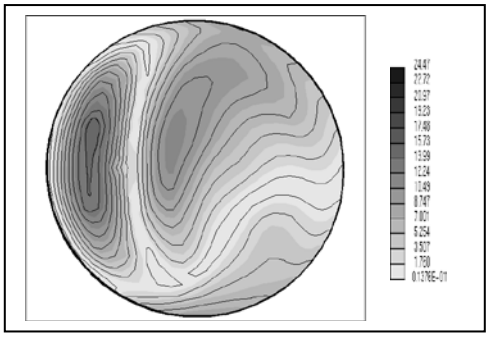

d

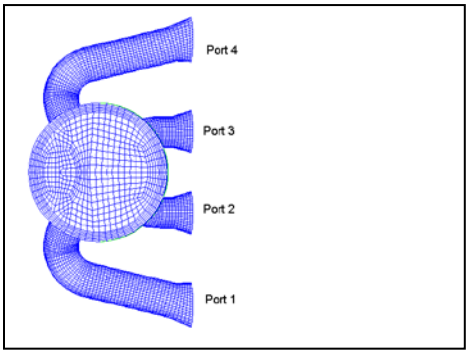

h

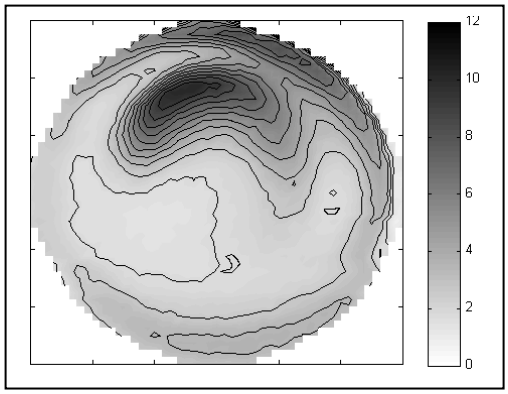

a

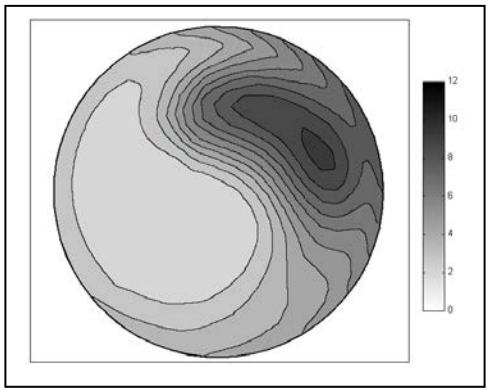

b

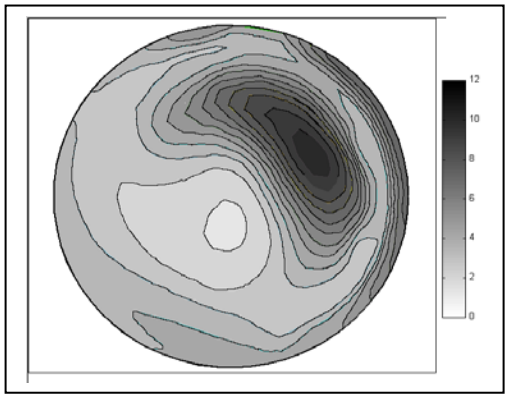

c

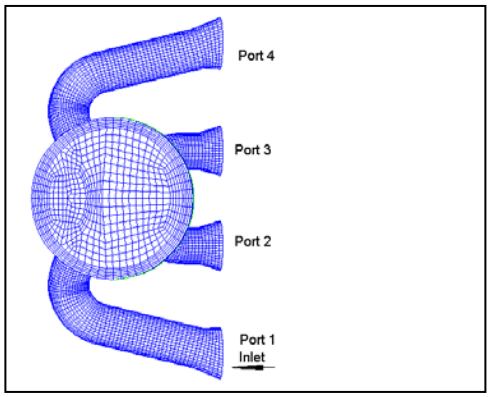

d

Figure 5 .